PIXE and EMP analyses of volcanites from Nea Kameni (Aegean Sea, Greece).

Mikrochim. Acta 114/115, 441–452 (1994)

Mikrochimica Acta

PIXE and EMP Analyses of Volcanites from Nea Kameni Island (Aegean Sea, Greece)

Alba P. Santo[1,*,**], John D. Mac Arthur[2], and Piero Manetti[3]

[1] Department of Earth and Planetary Science, Harvard University, Cambridge, U.S.A.
[2] Department of Physics, Queen's University, Kingston, Canada
[3] Dipartimento di Scienze della Terra, Universita' di Firenze, Italy

Abstract. The major and trace element compositions of several minerals and their surrounding groundmass in the volcanic rocks from the post-caldera Nea-Kameni island of the Santorini volcanic complex, Aegean Sea, have been determined, in-situ with particle-induced X-ray emission (PIXE) and wavelength dispersive X-ray analysis with an electron microprobe (EMP).

The lavas are typically calc-alkaline dacites. All samples are porphyritic with a phenocryst mineralogy dominated by plagioclase, augite, hyperstene and Ti-magnetite. The phenocrysts range in size from 200 μm to 2.5 mm.

The PIXE and EMP analyses were done on sections polished with diamond paste. They were sufficiently thick (≈ 100 μm) to stop the 2.7 MeV protons used for the analysis and yet thin enough for individual minerals to be seen with transmitted light. The specific minerals and groundmass areas to be analyzed had been selected and marked through conventional microscopic examination prior to analysis.

Solid/liquid partition coefficients, which depend much less significantly on the method for determining the concentrations, were calculated from the element abundances in phenocrysts and corresponding groundmass.

Key words: external PIXE, EMP, volcanic rocks, partition coefficients.

During the past few years, PIXE with a proton microprobe has been applied in several disciplines including the earth sciences for the measurement of trace elements in materials in a similar fashion to that of the electron microprobe which measures the major elements. Work in the Earth Sciences has been reviewed recently [1–4] while analyses of the major and trace elements in silicate rocks have been reported [5, 6].

Compared with other analytical methods, the multielemental, in-situ, high sensitivity (≈ 1 ppm) PIXE technique has definite advantages for the measurement of

* Permanent address: Dipartimento di Scienze della Terra, Via La Pira 4, I-50121 Firenze, Italy
** To whom correspondence should be addressed

trace-element abundances in magmatic rocks. The concentrations deduced with this technique represent the first step in the understanding of how the different chemical elements are partitioned between the solid and liquid phases during magma crystallization. Earlier experiments [7, 8] dealt with the determination of trace-element abundances in the groundmass and phenocrysts in volcanic rocks from the Aeolian islands (South Tyrrhenian Sea, Italy). From the data obtained in those experiments, solid/liquid partition coefficients ($K_{s/l}$) were deduced simply and quickly. Knowledge of these coefficients is essential to constrain quantitatively the magma evolution processes. Because the value of $K_{s/l}$ depends significantly on several factors (e.g. temperature and pressure) during magma crystallization, the measurement of trace element abundances directly in the rocks under investigation is highly desirable.

In the present work we have applied the PIXE technique to the study of the Nea Kameni volcanic rocks from the Santorini complex (Greece). The combination of the electron microprobe and PIXE measurements has proven to be very suitable for obtaining the major- and trace-element abundances in phenocrysts and groundmass of the rocks. Since there is a lack of such phenocryst/matrix partitioning data in the literature for these volcanic products, these analyses should help to fill this gap and possibly allow quantitative tests of evolutionary models of the magmas to be carried out.

Volcanological and Petrological Outline

The Santorini volcanic complex is part of the Aegean island arc. The volcanic activity along this arc started about 3 million years ago [9] and it is considered to be related to the subduction of the African plate beneath the Aegean microplate [10]. Santorini consists of five islands, Thera, Therasia, Aspronisi, Palea Kameni and Nea Kameni. The first three islands form a broken semicircular caldera 370 m deep [11] while Palea Kameni and Nea Kameni rise from the caldera centre and represent the sites of still active volcanism.

The Santorini rocks belong to the calc-alkaline series and they range continuously from basalts to dacites, rhyodacites and rhyolites [11, 12].

This study deals only with the post-caldera lavas from Nea Kameni. This island has resulted from several intermittent eruptions between 1570 and 1950 [11]. The Nea Kameni volcanics have holocrystalline or hypocrystalline porphyritic textures with phenocrysts and microphenocrysts of plagioclase, clinopyroxene, orthopy-

Table 1. Modal analyses (volume %) of the Nea Kameni rocks

	TH8	TH4	TH6	TH7	TH2	TH5	TH1	TH3
Plg	18.4	17.2	15.2	11.4	13.9	17.7	10.8	10.9
Opx	1.3	2.1	1.9	1.2	2.1	2.5	1.7	2.2
Cpx	1.0	2.1	1.6	0.7	1.1	0.8	1.1	0.9
Ox	1.2	1.7	1.2	0.7	1.1	2.3	1.0	1.1
Gdm	78.1	76.9	80.1	86.0	81.8	76.7	85.4	84.9

Plg = plagioclase, Opx = orthopyroxene, Cpx = clinopyroxene, Ox = oxide, Gdm = groundmass.

roxene and Fe-oxides set in a fine-grained groundmass which contains abundant plagioclase microlites. Modal compositions, determined by point counting (Table 1) show that plagioclase is by far the most abundant phenocryst phase followed by pyroxenes. Plagioclase is generally euhedral and variously twinned. Clinopyroxene, orthopyroxene and Fe-oxides occur as euhedral, subhedral to anhedral crystals. Some of the euhedral crystals may represent xenocrysts. Finally, xenocrysts of resorbed olivine, clearly not in equilibrium with the liquid, are present in a few samples.

Experimental

For the present study, eight samples, covering all the eruptions between 1570 and the present with the exception of the 1710 lava flows, were selected.

Whole rocks were analyzed by conventional wet chemical techniques (Na_2O, MgO, P_2O_5, FeO, L.O.I.) and by X-ray fluorescence using several international rock standards for sensitivity calibration. Precisions better than 5% for Rb and Sr and better than 10% for Zr, Y, Nb and Ni were obtained.

The determination of the abundances of the major elements in the mineral phases and the groundmass was done at the Department of Earth and Planetary Science, Harvard University, with a Cameca MBX electron microprobe equipped with a Tracor Northern TN-1310 WDS system and operating at 15 kV and 15 nA. Corrections for matrix effects were done according to the method of Bence and Albee [13]. The groundmass was analyzed using a ≈ 100 μm large beam to average over the small grains of the groundmass itself. For each sample, several areas were analyzed; since the measurements from all spots produced reproducible abundances, they were averaged and taken as representative of the groundmass composition.

The same mineral phases and the groundmass were also analyzed with the external micro-PIXE facility at the Department of Physics, Queen's University. For these measurements, the thin polished sections were examined with protons of energy 2.7 MeV and a current of a few nA for 1000 seconds. The capability of performing the measurements in an external environment results in easier handling of the samples and a smaller risk of beam bombardment-induced damage to the sections. The samples were viewed from the rear with a microscope-camera so that it was possible to position the beam on a chosen phenocryst or groundmass area.

In-situ, multielemental PIXE analysis has distinct advantages for the measurement of the groundmass composition over traditional methods which involve mineral separation from the matrix or a "computational" approach based on the counting point analyses of the rocks [14]. It gives as good results as the latter [8] but is considerably less time consuming. To be effective, the more homogeneous and small-grain-sized areas of the groundmass must be measured with a beam, small enough in diameter to avoid hitting phenocrysts but large enough to determine the average composition. In these experiments, a beam of 200 μm diameter was chosen as the best compromise between these requirements. Several spots on each sample of groundmass were analyzed. As the analyses showed good reproducibility, they were considered representative of the groundmass composition and averaged.

Only phenocrysts with visible dimensions greater than 200 μm were selected for analysis with the hope that the depth of the phenocryst was at least greater than the range of 2.7 MeV protons which is approximately 60 μm in the phenocrysts. The beam diameter for these experiments was 100 μm.

Two Si(Li) detectors were used to observe the X-rays produced: one of size 13 mm^2 with a resolution of 150 eV FWHM at 5.9 KeV and without attenuator in front of it, observed the intense low energy X-rays from elements with atomic number $Z \geq 12$ and the second one of area 80 mm^2 with a resolution of 180 eV FWHM at 5.9 KeV and with an aluminum absorber to attenuate the intense low-energy X-rays. The latter was used to detect the lower-intensity, higher-energy X-rays from elements such as Rb, Sr, etc. A typical spectrum recorded with this detector is presented in Fig. 1 which illustrates the high sensitivity of the method.

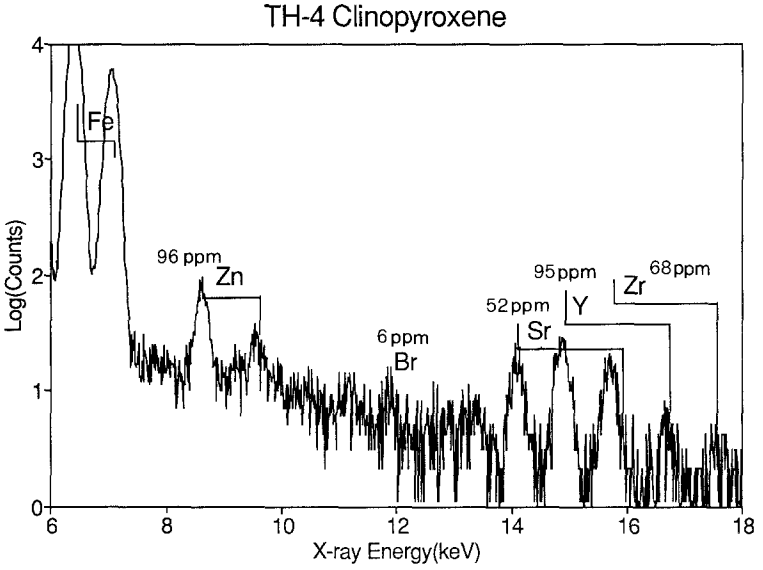

Fig. 1. Typical X-ray spectrum referring to a PIXE measurement of a clinopyroxene from TH4

The counting rates for each element in each spectrum were determined with a spectrum analysis program which utilizes a gaussian peak shape for each line in an element's spectrum and the X-ray relative intensities of Salem et al. [15] modified for any absorber positioned between the target and the detector.

To convert the counting rates to concentrations, matrix effects were computed for the phenocrysts and the groundmass based on their major element composition determined with the electron microprobe. For each element in the different matrices, the relative X-ray production was computed as outlined in MacArthur and Ma [1], employing the ionization cross sections of Cohen and Harrington [16], the fluorescence yields of Krause [17], the stopping powers of Andersen and Ziegler [18] and the relative line intensities of Salem et al. [15].

The product of the incident flux and the solid angle for each detector and each spectrum was determined from the counting rate of an intense line from an element of known concentration. For the detector recording the X-rays from the low atomic mass elements (up to and including Zn), the concentration of Si from the EMP analyses was used. For the bigger detector, the concentration of Fe, as deduced from the measurements with the smaller detector, was used. Thus, all concentrations have been determined relative to the concentration determined for Si in the EMP experiments.

As a check on the correctness of this procedure, the concentrations of several elements determined with the small detector, such as K and Ca, could be compared to values known from EMP analyses. Although differences were observed, these were generally within the accuracy of the determinations which is about 10% because of uncertainties in the data-base and spectrum analysis program.

Variations in the element concentrations from the several spots on the groundmass were less than 10% for all the elements determined with the small detector. The statistical uncertainty with the larger detector was high in the single spectra; consequently, they were added together to improve the statistical precision of the elements of low concentration. Upper limits on the trace element concentrations in Table 5 correspond to a 99% confidence level.

Results and Discussion

The major and minor ($>0.1\%$) and trace ($<1000\ \mu g/g$) element abundances of the rocks (Table 2) from the Nea Kameni post-caldera lavas are typical of calc-alkaline

Table 2. Major (wt%) and trace (μg/g) element analyses of the Nea Kameni rocks

	TH8	TH4	TH6	TH7	TH2	TH5	TH1	TH3
SiO_2	64.3	64.6	65.0	65.2	65.4	65.5	65.9	66.4
TiO_2	0.71	0.85	0.82	0.83	0.81	0.79	0.81	0.75
Al_2O_3	14.8	15.1	15.2	15.3	15.3	15.3	15.1	15.0
FeO	4.3	5.4	5.0	5.1	4.9	4.9	4.9	4.6
MnO	0.13	0.16	0.15	0.15	0.15	0.15	0.15	0.14
MgO	1.2	1.5	1.4	1.4	1.4	1.4	1.2	1.3
CaO	3.3	3.9	3.7	3.6	3.6	13.6	3.3	3.3
Na_2O	5.2	5.1	5.2	5.2	5.2	5.2	5.2	5.3
K_2O	1.8	1.8	1.8	1.8	1.8	1.8	1.9	1.8
P_2O_5	0.14	0.14	0.15	0.15	0.15	0.15	0.15	0.14
L.O.I.	3.5	1.2	1.3	1.2	1.1	1.2	1.3	1.2
Ni	3	4	4	3	3	3	4	4
Rb	62	60	64	59	60	60	66	62
Sr	153	167	167	167	166	163	157	156
Y	34	36	37	36	34	36	38	37
Zr	218	214	227	221	211	220	242	226
Nb	8	8	9	8	7	8	20	9

dacites. The composition of these lavas has remained approximately constant over a long period of time; in fact, the analyzed samples from the different eruptive cycles show a restricted range of composition (from 64.3 to 66.4 wt% SiO_2), as already observed by previous workers [19, 20].

Representative major element data for the mineral phases and the corresponding groundmass are given in Tables 3 and 4. The minerals show the composition typically found in minerals from the island arc rocks [21, 22]. Significant differences in the composition of the minerals belonging to the different samples have not been detected. Plagioclases have only slightly variable anorthite content (43–57%) and they exhibit a not remarkable, normal or reverse zoning. Clinopyroxenes are always augitic in composition and they are practically unzoned. Orthopyroxenes show constant composition as well, ranging from 60% to 64% enstatite content. Also in this mineral, there is no noticeable zoning. Finally, the opaque minerals consist of Ti-magnetites. Xenocrysts of plagioclase, pyroxene, olivine and oxides are ubiquitous, displaying a different composition from that of the other phenocrysts.

Some major element data from the whole rocks and the groundmass are reported in Fig. 2, which shows variation diagrams versus SiO_2 used as a differentiation index. As expected, larger silica contents are always observed in the groundmass than in the corresponding whole rocks. Variation trends however are similar for groundmass and whole rocks: Al_2O_3, TiO_2, CaO, MgO and FeO decrease with differentiation whereas Na_2O and K_2O show an increase with silica despite the large scattering in the data. These trends are clearly related to the phenocrysts' separation during magma evolution.

The measured trace element abundances in the phenocrysts from the Nea Kameni rocks are comparable with those generally found in similar island arc rocks,

Table 3. Representative EMP analyses (wt%) of minerals from the Nea Kameni rocks

	Plagioclase									
	TH8 phcr		TH6	TH7 phcr		TH2	TH1 phcr		TH3 phcr	
	rim	core	mphcr	rim	core	mphcr	rim	core	rim	core
SiO_2	55.8	55.1	53.8	54.5	54.8	56.5	55.7	54.2	55.7	55.7
Al_2O_3	27.9	27.5	28.5	28.4	28.2	27.7	27.8	28.4	28.3	28.2
FeO	0.44	0.51	0.66	0.51	0.57	0.51	0.42	0.46	0.49	0.49
CaO	10.2	10.2	11.3	11.2	10.7	10.1	10.2	11.1	10.1	10.4
Na_2O	5.6	5.7	4.9	5.1	5.2	5.4	5.6	5.1	5.6	5.4
K_2O	0.17	0.17	0.13	0.13	0.14	0.18	—	—	—	0.17
Sum	100.11	99.18	99.29	99.84	99.61	100.39	99.72	99.26	100.19	100.36
An	50.0	49.5	55.3	54.6	52.9	50.4	50.2	54.4	49.4	51.0
Ab	49.0	49.5	43.9	44.6	46.2	48.5	49.8	45.6	49.6	48.0
Or	1.0	1.0	0.80	0.80	0.90	1.1	—	—	1.0	1.0
	Clinopyroxene									
	TH4	TH6 phcr		TH7 phcr		TH2	TH1 phcr		TH3 mphcr	
	mphcr	rim	core	rim	core	mphcr	rim	core	rim	core
SiO_2	51.7	52.4	52.3	51.9	50.4	51.9	50.0	52.1	51.5	51.8
TiO_2	0.47	0.43	0.47	0.57	0.89	0.46	0.89	0.38	0.46	0.54
Al_2O_3	1.5	1.3	1.3	1.8	2.8	1.5	2.9	1.2	1.4	1.7
Fe_2O_3	2.1	1.5	1.1	1.4	2.9	1.5	3.2	1.9	1.7	1.7
Cr_2O_3	—	—	—	—	—	—	0.03	0.04	—	—
FeO	9.0	9.3	9.4	8.9	8.4	8.5	8.9	10.5	8.7	8.6
MnO	0.61	0.60	0.52	0.52	0.54	0.53	0.59	0.75	0.54	0.57
MgO	14.5	14.8	14.7	14.8	14.3	14.9	13.7	14.4	14.6	14.6
CaO	19.7	19.8	19.9	19.7	19.6	19.9	19.6	19.0	19.8	20.0
Na_2O	0.33	0.32	0.29	0.30	0.34	0.29	0.36	0.27	0.30	0.33
Sum	99.91	100.45	99.98	99.89	100.17	99.48	100.17	100.54	99.00	99.84
Wol	40.3	40.3	40.8	40.5	40.6	40.8	40.5	38.5	40.8	41.0
Ens	41.3	41.8	41.8	42.4	40.9	42.7	39.4	40.9	41.8	41.8
Fer	18.4	17.9	17.4	17.1	18.5	16.5	20.1	20.5	17.4	17.2

Table 3 (cont.)

	Orthopyroxene									Oxide	
	TH8	TH6 mphcr		TH7	TH2 phcr		TH3 phcr			TH8	TH3
	mphcr	rim	core	mphcr	rim	core	rim	core			
SiO_2	52.2	53.3	53.2	53.0	53.0	52.8	52.8	52.0		0.11	0.11
TiO_2	0.32	0.29	0.27	0.26	0.30	0.29	0.26	0.34		17.1	15.8
Al_2O_3	0.95	0.78	0.74	0.61	0.71	0.79	0.64	1.9		1.4	2.2
Fe_2O_3	2.1	1.7	2.2	1.9	1.2	1.9	1.5	2.5		34.6	36.2
Cr_2O_3	—	—	—	—	—	—	—	—		0.04	0.08
FeO	20.9	18.9	18.9	19.1	19.7	19.6	21.1	19.0		44.4	42.9
MnO	1.0	0.95	0.88	0.99	1.1	1.0	1.6	0.84		1.0	0.8
MgO	21.5	23.6	23.5	23.2	22.8	22.7	21.9	22.4		1.2	1.6
CaO	1.8	1.5	1.5	1.5	1.6	1.6	1.6	2.0		—	—
Na_2O	—	—	0.03	—	0.03	0.03	0.03	0.04		—	—
Sum	100.77	101.02	101.22	100.56	100.44	100.71	100.93	101.02		99.80	99.70
Wol	3.5	3.0	3.0	3.0	3.2	3.1	3.1	4.0	Usp	47.9	44.3
Ens	59.4	64.4	63.9	63.6	62.9	62.5	60.3	61.8			
Fer	37.1	32.6	33.1	33.4	33.9	34.4	36.6	34.2			

phcr = phenocryst, mphcr = microphenocryst, An = anorthite, Ab = albite, Or = orthoclase, Wol = wollastonite, Ens = enstatite, Fer = ferrosilite, Usp = ulvosphinel.

Table 4. EMP major element analyses (wt%) of the groundmasses

	TH8	TH4	TH6	TH7	TH2	TH5	TH1	TH3
SiO_2	69.5	70.3	69.4	68.4	71.3	70.9	68.5	71.6
TiO_2	0.48	0.78	0.56	0.72	0.52	0.52	0.82	0.27
Al_2O_3	15.1	14.1	15.4	15.3	14.3	14.7	14.8	15.3
FeO	2.9	3.6	3.0	3.7	2.8	2.4	4.3	1.9
MnO	0.14	0.14	0.12	0.10	0.11	0.06	0.12	0.08
MgO	0.44	0.53	0.51	0.66	0.38	0.23	0.78	0.17
CaO	2.7	2.4	3.0	3.1	2.4	2.5	2.9	2.7
Na_2O	5.5	5.2	5.4	5.4	5.2	5.7	5.3	5.5
K_2O	3.2	2.9	2.6	2.6	2.9	2.9	2.6	2.5

e.g. [7, 23]. Even though many values are given as limits only, the compositions of the same mineral phases from the different samples are in general agreement. The only discordant compositions are in the plagioclase of TH4 and the clinopyroxene and orthopyroxene of TH8; furthermore, the concentration of the major elements in these minerals differs from that of the other phenocrysts suggesting that these grains are of xenocrystic nature. The presence of xenocrysts of all the main mineral phases within these rocks has been also observed by Barton and Huijsmans [19], who interpreted these xenocrysts as disaggregation products of the cognate xenoliths.

The trace element composition of the groundmass displays only small differences among the analyzed samples. In comparison to the whole rock analyses, Ni and Nb abundances in the groundmass, although always below the detection limits of these experiments, are consistent with the low values found in the corresponding whole rock samples. Sr also shows a distinct decrease in the amount detected in the groundmass compared to the whole rock analyses. However, no difference is observed in the amount of Rb and Y between the groundmass and whole rock analyses. Finally, Zr content in the groundmass is comparable to that in the corresponding whole rock.

Concluding Remarks

The obvious application of these data is for the calculation of solid/liquid partition coefficients, $K_{s/l}$, for use in magmatological modelling. This coefficient is defined as the ratio of the element's abundance in the mineral to the abundance in the liquid phase from which the mineral crystallizes. In general, the $K_{s/l}$ for each mineral phase depends on many parameters, temperature, pressure, O_2 fugacity, etc., during mineral crystallization [24, 25]. However, when the element abundances in the mineral phases and the groundmass can be measured directly, these coefficients can be simply obtained as the ratio of the abundance in the phenocryst to that in the groundmass [26]. To be meaningful, the latter must be assumed to be a true record of the coexisting liquid phase at the time of mineral crystallization. Consequently, a kinetic equilibrium between phenocrysts and the coexisting groundmass must be assumed.

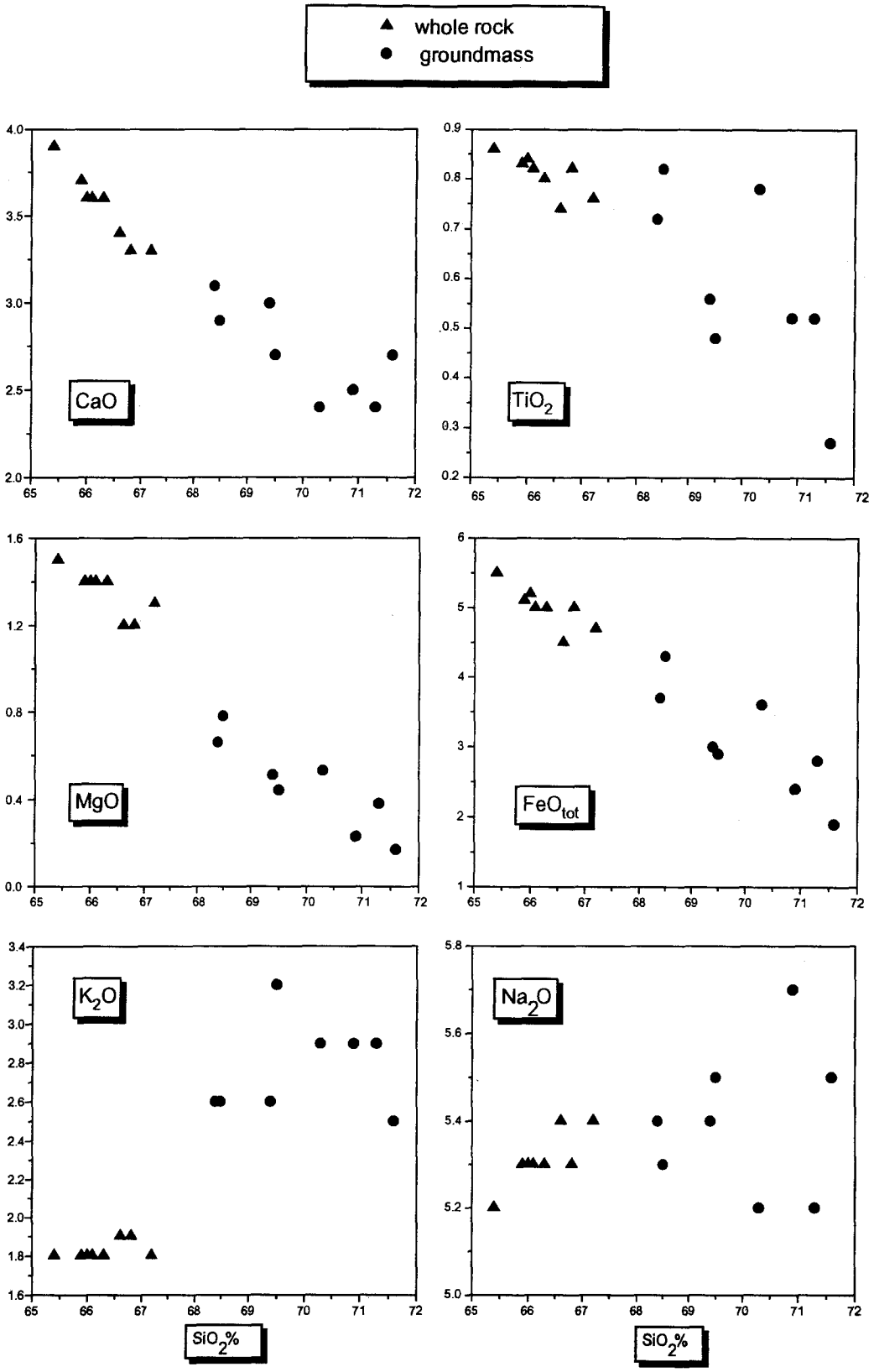

Fig. 2. Variation diagrams of major elements (wt%) against silica. The data are plotted on water-free basis

Table 5. Representative PIXE trace element analyses (μg/g)

	Plagioclase							
	TH8	TH4	TH6	TH7	TH2	TH5	TH1	TH3
		*						
Ni	<3	<3	<3	<3	<3	<3	<3	<3
Cu	1	224	2	4	3	3	13	5
Zn	11	<5	14	17	8	14	27	23
Rb	<3	<3	<3	<3	<3	<3	<3	<3
Sr	662	437	710	618	496	650	700	575
Y	<4	<4	<4	<4	<4	<4	<4	<4
Zr	<20	<20	<20	<20	<20	<20	<20	<20
Nb	<5	<5	<5	<5	<5	<5	<5	<5

	Clinopyroxene						Orthopyroxene				
	TH8	TH4	TH6	TH7	TH2	TH5	TH8	TH4	TH7	TH2	TH3
	*						*				
Ni	45	<5	<5	<5	<5	<5	<15	<15	<15	<15	17
Cu	<5	<5	<5	<5	<5	<5	<6	<6	7	<6	7
Zn	21	96	88	87	100	86	254	262	276	260	312
Rb	—	9	<8	<8	<8	<8	12	29	16	20	30
Sr	17	52	18	14	22	20	14	18	24	12	11
Y	11	95	55	46	64	60	13	10	24	8	<5
Zr	6	68	26	40	33	32	44	28	29	3	9
Nb	<10	<10	<10	<10	<10	<10	<8	<8	<8	<8	<8

	Groundmass							
	TH8	TH4	TH6	TH7	TH2	TH5	TH1	TH3
Ni	<6	<6	<6	<6	<6	<6	<6	<6
Cu	10	14	10	10	12	10	14	10
Zn	80	66	64	72	64	66	80	66
Rb	65	60	56	64	60	67	70	60
Sr	95	110	102	114	116	104	118	110
Y	40	39	36	35	32	32	37	34
Zr	240	196	196	226	193	200	238	203
Nb	<10	<10	<10	<10	<10	<10	<10	<10

* Xenocrysts.

In the present study, the analyzed phenocrysts showed no petrographic or chemical (EMP analyses) evidence of zoning; hence we concluded that kinetic equilibrium existed between the minerals and the liquid. Lack of zoning in the Nea Kameni phenocrysts also means that, with the larger beams used for PIXE analysis, the values obtained represent the actual phenocryst's composition. Clearly, no

Table 6. Representative trace element partition coefficients

	Plagioclase						
	TH8	TH6	TH7	TH2	TH5	TH1	TH3
Cu	0.10	0.20	0.40	0.25	0.30	0.93	0.50
Zn	0.14	0.22	0.24	0.13	0.21	0.34	0.35
Rb	<0.05	<0.05	<0.05	<0.05	<0.04	<0.04	<0.05
Sr	7.0	7.0	5.4	4.3	6.3	5.9	5.2
Y	<0.10	<0.11	<0.11	<0.13	<0.13	<0.11	<0.12
Zr	<0.08	<0.10	<0.09	<0.10	<0.10	<0.08	<0.10

	Clinopyroxene					Orthopyroxene			
	TH4	TH6	TH7	TH2	TH5	TH4	TH7	TH2	TH3
Cu	0.36	0.50	<0.50	<0.40	<0.50	<0.40	0.70	<0.50	0.70
Zn	1.5	1.4	1.2	1.6	1.3	3.9	3.8	4.1	4.7
Rb	0.15	<0.14	<0.13	<0.13	<0.12	0.48	0.25	0.33	0.50
Sr	0.50	0.18	0.12	0.19	0.19	0.16	0.21	0.10	0.10
Y	2.4	1.5	1.3	2.0	1.9	0.26	0.69	0.25	<0.15
Zr	0.30	0.13	0.18	0.17	0.16	0.14	0.13	0.02	0.04

partition coefficient can be calculated in the case of xenocrysts due to a lack of knowledge of their coexisting liquid composition. Consequently, considerable care must be taken in analyzing rocks which contain grains of xenocrystic nature.

Table 6 reports values of $K_{s/l}$ obtained from the concentrations. With few exceptions the values are similar to those reported in the literature for minerals from the same type of rocks [7, 21, 22]. Generally, they fall in the range of $K_{s/l}$ used by Barton and Huijsmans [19] to model the crystal-liquid differentiation processes for the Nea Kameni rocks. However, since the $K_{s/l}$ of Table 6 were obtained directly on those rocks, we suggest their use, instead of values of $K_{s/l}$ from the literature, in order to test the processes involved during the differentiation of the rocks studied.

From the data reported it follows that the PIXE technique can be extremely suitable for the analysis of many trace-element abundances at concentrations as low as a few ppm. Moreover, the combined use of PIXE and EMP represents a particularly helpful procedure for the determination of major- and trace-element composition of mineral phases and groundmass.

Acknowledgements. This research is part of the EC project on volcanic risk (Santorini Volcano Laboratory). The authors would like to thank prof. P. A. Mando', Universita' di Firenze, for critical reading of the manuscript and dr. D. Lange, Harvard University, for technical assistance during EMP analyses. The Nature Science and Engineering Research Council of Canada and the Advisory Research Council of Queen's University is acknowledged. Financial support was also provided by Italian C.N.R. NATO fellowship granted to A.P.S.

References

[1] J. D. MacArthur, X.-P. Ma, *Intr. J. Pixe* **1991**, *1*, 311.
[2] H. J. Annegarn, S. Bauman, *Nucl. Instr. Meth.* **1990**, *B49*, 264.
[3] S. H. Sie, C. G. Ryan, D. R. Cousens, W. L. Griffin, *Nucl. Instr. Meth.* **1990**, *B45*, 604.
[4] J. L. Campbell, J. A. Maxwell, W. L. Teasdale, J.-X. Wang, L. J. Cabri, *Nucl. Instr. Meth.* **1990**, *B44*, 347.
[5] J. D. MacArthur, X.-P. Ma, G. R. Palmer, A. J. Anderson, A. H Clark, *Nucl. Instr. Meth.* **1990**, *B45*, 322.
[6] T. H. Green, S. H. Sie, C. G. Ryan, D. R. Cousens, *Chem. Geol.* **1989**, *74*, 201.
[7] A. P. Santo, P. A. Mandò, A. Peccerillo, *Per. Mineral.* **1991**, *60*, 65.
[8] A. P. Santo, A. Peccerillo, P. Del Carmine, F. Lucarelli, J. D. MacArthur, P. A. Mandò, *Nucl. Instr. Meth.* **1992**, *B64*, 517.
[9] M. Fytikas, O. Giuliani, F. Innocenti, G. Marinelli, R. Mazzuoli, *Tectonophysics* **1976**, *31*, 29.
[10] D. Ninkovitch, J. D. Hays, *Earth Planet. Sci. Lett.* **1972**, *16*, 331.
[11] S. Kalogeropoulos, S. Paritsis, *Thera and the Aegean World, Vol. III*, The Thera Foundation, 1990, p. 164.
[12] M. Fytikas, F. Innocenti, P. Manetti, R. Mazzuoli, A. Peccerillo, L. Villari, *Geol. Soc. Lond.* **1984**, *17*, 687.
[13] A. E. Bence, A. L. Albee, *J. Geol.* **1968**, *6*, 382.
[14] W. P. Nash, H. R. Crecraft, *Geochim. Cosmochim. Acta* **1985**, *49*, 2309.
[15] S. I. Salem, S. L. Panossian, R. A. Krause, *At. Data Nucl. Data Tables* **1974**, *14*, 91.
[16] D. D. Cohen, M. Harrigan, *At. Data Nucl. Data Tables* **1986**, *34*, 393.
[17] M. O. Krause, *J. Phys. Chem. Ref. Data* **1979**, *8*, 307.
[18] H. H. Andersen, J. F. Ziegler, *Hydrogen: The Stopping Powers and Ranges in all Elements*, Pergamon, New York, 1977.
[19] M. Barton, J. P. P. Huijsmans, *Contrib. Mineral. Petrol.* **1986**, *94*, 472.
[20] L. Briqueu, J. R. Lancelot, *J. Volcanol. Geotherm. Res.* **1984**, *20*, 41.
[21] A. Ewart, in: Andesites (R. S. Thorpe, ed.), Wiley, New York, 1982.
[22] J. B. Gill, *Orogenic Andesites and Plate Tectonics*, Springer, Berlin Heidelberg New York, 1981.
[23] L. Francalanci, *N. Jb. Miner. Abhr.* **1989**, *160*, 229.
[24] B. O. Mysen, *Carnegie Inst. Wash. Yearb.* **1976**, *75*, 662.
[25] E. B. Watson, *Geochim. Cosmochim. Acta* **1985**, *49*, 917.
[26] G. Mahood, W. Hildreth, *Geochim. Cosmochim. Acta* **1983**, *47*, 11.